Energy Transfer between Dark Matter and Gas during Collisions

by

Starling Cox

A THESIS SUBMITTED IN PARTIAL FULFILMENT OF
THE REQUIREMENTS FOR THE DEGREE OF

BACHELOR OF SCIENCE

in

Honours Astrophysics

(Department of Astronomy and Physics, Dr. Robert J. Thacker supervising faculty)

.....
.....
.....
.....
.....

SAINT MARY'S UNIVERSITY

April 19, 2024

Abstract

Energy Transfer between Dark Matter and Gas during Collisions

Using the simulation code GIZMO, two different configurations of dark matter and gas were collided at three different resolutions in order to study the energy transfer between the dark matter and gas. The first configuration is of two dark matter halos offset from a central gas distribution. Energy was transferred from the dark matter into the gas, and an increase in the gas temperature and kinetic energy occurred. The second configuration is of two mixed gas and dark matter halos offset from each other. This collision sees a spike in temperature initially, and then an adiabatic expansion and cooling that leaves the gas cooler then it was initially, while also seeing an increase in kinetic energy. When normalized by taking the energy values as a ratio of the initial total energy, the energy transfer from the dark matter to the gas ended up being roughly the same value (0.025) for the two collisions, at the highest resolutions. by *Starling Cox*

submitted on April 19, 2024:

Contents

List of Figures

List of Tables

Chapter 1

INTRODUCTION

1.1 General Review of Relevant Cosmology

The beginning of modern cosmology can arguably be traced back to Hubble and Humason (11) (7) identifying the distances to other galaxies. Scale and distance in cosmology are determined by the luminosity and spectral properties of light reaching earth from distant stars and galaxies. By determining the red or blue-shift of light from distant objects due to the Doppler effect, it can be determined whether they are travelling towards or away from us, the observer (11). Most distant objects are red-shifted, and as first demonstrated by Hubble, in general the more red-shifted they are, the farther away they are. In other words, distant objects are moving away from us, and the more distant they are, the faster they are moving away.

However, this recession away from us is not because we have any special place in the universe; rather it is hypothesized that this is happening at every point in space, and is due to the homogeneous and isotropic expansion of the universe (11). Thus on cosmological scales, every point in space is gradually expanding away from every other point. By quantifying this expansion, using Cepheid variable stars as "standard candles," Hubble and Humason found there was a relation between the redshift of

galaxies and their distance from us, given by Hubble's Law: (11)

$$v = H_0 r$$

Where v is the velocity of the galaxy away from us, determined by red-shift, r is proper distance, and H_0 is Hubble's Constant, found to be 69.8 $km \cdot s^{-1} \cdot Mpc^{-1}$ in the local universe. (5)

This redshift-distance relation was used by the 2dF Galaxy Survey team to map a slice of the visible universe (3), which, by representing each galaxy as a point, gives a depiction of the distribution of galaxies. The survey mapped angular slices of the night sky and included approximately 250,000 galaxies. The slice of the galaxy distribution appears as a giant web-like structure with areas of higher and lower density matter. (3) The Sloan Digital Sky Survey (or SDSS) is a more recent effort to map the visible universe, and also uses redshift and baryon acoustic oscillations, just on much larger scales. SDSS has mapped roughly 930,000 galaxies and 1.3 million objects so far, with galaxies being picked up beyond a redshift of 0.7, and quasars beyond a redshift of 6. (4)

In the hot Big Bang theory (11), the universe has been expanding and cooling since it's moment of creation. While still a matter of research, there appears to have been an early moment of expansion that was incredibly fast, the so-called inflationary epoch (which only lasted for about 10^{-32} seconds) (11), meaning the smallest quantum fluctuations in matter in the first fractions of a second after the Big Bang are inflated

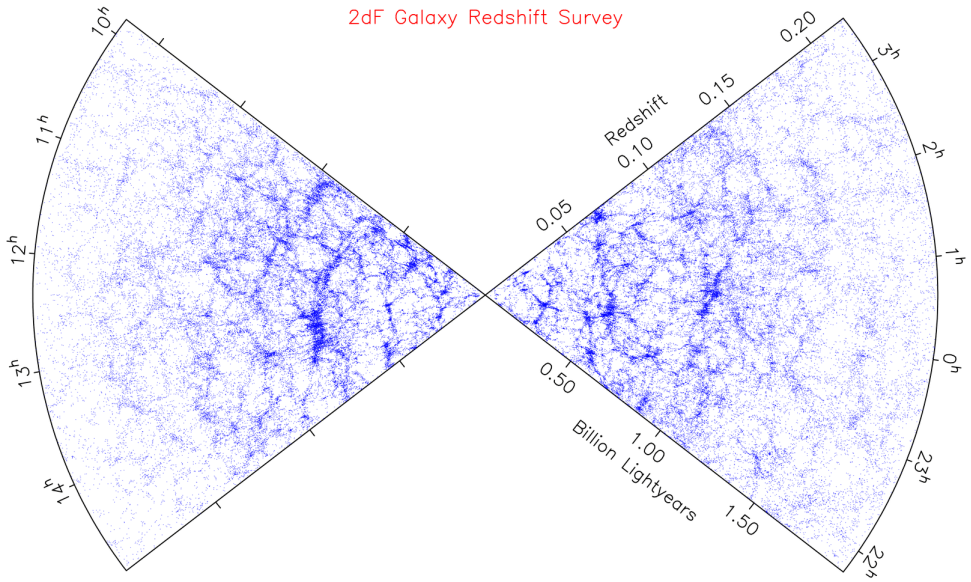

Figure 1.1: Slice of the distribution of galaxies from the 2dF Galaxy Redshift Survey

in size to be the cause for fluctuations in matter density on a grand cosmological scale (11).

> Great superclusters from tiny quantum fluctuations grow.
>
> - Barbara Ryden, Introduction to Cosmology

These areas of higher or lower density can be seen in the Cosmic Microwave Background. The cosmic microwave background (CMB) is semi-uniform background radiation that can be seen between cosmological objects such as galaxies and clusters which are essentially foreground objects in front of the CMB. The CMB is sourced from the surface of last scattering during the era of recombination, roughly 400,000 years after the Big Bang, when the universe cooled from an opaque soup of hot, dense plasma and formed the first atoms (15). It gives us a direct look into the early universe, and was the starting point for the structure of the universe we see today. Under the mutual attraction of gravity, areas of higher density drew more and more

matter from the lower density areas. The first stars formed within the first galaxies, these first galaxies merged to former larger ones, and then clusters of galaxies formed, and finally super clusters. This process of progressively forming larger structures is known as "hierarchical clustering." The major structure of the universe is made up of these galaxies, clusters, and super-clusters, which contain the vast majority of the mass of the universe in a form that does not seem to interact with electromagnetic radiation, and is known as dark matter. Studying what matter galaxies are composed of, therefore gives us insight into what the universe as a whole is composed of (11).

One of the most central mysteries in cosmology is the existence of dark matter. In the 1930s Fritz Zwicky studied (1) the dynamics of galaxy clusters, and this is when it was first suggested there is significantly more matter in the universe than is observable to us. The radial velocity of a wide variety of spiral galaxies have been studied, including our own, and unlike predicted by Kelpernian Rotation ($v \propto \frac{1}{R^2}$), the velocity stays relatively constant with radius (10). The mass of the galaxy predicted by mass-to-light ratios of stars and interstellar gas is less than would be required to keep the outermost matter gravitationally bound; i.e. to keep it from flying off into space. This suggests a massive dark matter halo that makes up approximately 80% of the galaxy's mass, far more then can be accounted for by visible matter. If our galaxy, and the spiral galaxies we've seen are typical, then most dark matter is non-baryonic dark matter and is likely a relic subatomic particle.

This means dark matter is a material that has mass, and interacts through gravitational forces with other matter, but does not interact through electrodynamic forces or thermodynamics. Given that it makes up approximately 80% of the mass in the universe, it has a profound impact on the dynamics of cosmological objects. Dark matter as of yet, can only be inferred through it's interactions with visible matter and the ways in which it shapes these dynamics. Direct detection in a laboratory setting remains elusive. Understanding the way dark matter and baryonic matter interact can give us a better understanding of dark matter, as well as the dynamics of cosmological growth.

1.2 Simulation methods

Galaxies and galaxy clusters can be computationally modeled as distributions of gas with "n" particles all interacting with each other through gravitation, fluid dynamics and thermal properties. The evolution of such coupled systems is determined by repeated solution cycles of force equations. Modeling them this way can allow us to simulate evolution from an initial state to a final one. For galaxy and cluster mergers, we can use computational methods to derive theoretical insight into dynamics. One of the by-products of creating these computer simulations is that they can be used to create "mock" visual observations, that can then be directly related to the underlying physics that created them. Providing a bridge between observation and theory.

The algorithms used are a solver for gravitation, and also hydrodynamics (for the gas particles). The algorithm used in our program, GIZMO, to solve for gravity is called Tree Particle-Mesh or "Tree-PM", and the hydrodynamics solver is called Lagrangian Meshless-Finite-Mass, or "MFM".

1.3 Thesis motivation

As previously discussed, galaxies and galaxy clusters are modeled as being made up of dark matter, gas, and stars. Energy transfer between dark matter and stars is fairly straightforward, due to the interactions being mediated solely by gravity. Dark matter particles are assumed to be able to pass through one another: called "collisionless." Interactions between dark matter and gas, however, are more complex. While the interaction between gas and dark matter is purely gravitational, the dynamics of these systems is also influenced by the hydrodynamics of the gas. Energy can transfer in the gas between potential, kinetic, and thermal components. It is currently unknown whether the energy transfer from dark matter to gas has an upper limit, or if energy can be pumped into the system repeatedly, being determined by the initial velocities and density profiles of the colliding objects.

Pearce et al published a paper in 1994 titled "Head on Mergers of Systems containing Gas" (9), where collisions between gravitating spheres of dark matter, dark matter and gas, as well as purely gas were studied. A literature search was done during the summer to identify if anyone had expanded the work undertaken in this paper.

However, most work since then focused on physically observable properties, like the x-ray radiation, rather then studying the fundamental physics of the gas. Computing power has increased significantly since this initial work in 1994, and we can improve and expand on these simulations with higher resolutions, as well as new scenarios for the collisions, including separating the gas from the dark matter as might possible, but admittedly rare since gravity pulls gas and dark matter mutually, in the universe.

Hence, we will be simulating collisions between dark matter separated from a central gas distribution, as well as dark matter and gas directly overlaid. As in Pearce et al (1994), these two distributions will be made with equal masses of gas and dark matter, although differently distributed. By separating the gas from the dark matter we create the possibility of the dark matter moving rapidly through the gas without the gas moving alongside the dark matter in the initial infall. To create a distribution of gas separate from the dark matter we will run simulations that evolve a gas sphere into a heated equilibrium state and then insert this distribution between dark matter distributions. We have used a well known collapse problem, the so-called Evrard (1994) "collapse (13)".

Chapter 2

METHODS

Simulations of collisions between various distributions of gas and dark matter were undertaken using the code GIZMO (6). The code used to set up the initial distributions of gas and dark matter was a mix of GalactICS code, as well as code developed for this project. The ball of hot gas at the centre of the distribution was created using a newly developed code and then run through an Evrard Collapse so that it would be in equilibrium for the simulations. Fraser Smith provided the dark matter and dark matter mixed with gas distributions, created to fit a NFW profile.

2.1 Setting up the Initial Conditions

There are two main distributions of dark matter and gas that were being tested. The first is two dark matter halos around a central gas distribution. For this distribution, a gas sphere was created using newly developed code and then added to the centre of a distribution of two halos of dark matter separated by a distance. (See Figure 2.4) This distribution needs the central gas to be in equilibrium before the start of the simulation, as otherwise it will begin to collapse under it's own weight. The second distribution is of the same two dark matter halos, but with the gas shifted and overlaid over their centres. (See Figure 2.5) The first distribution will be referred to as the "Central Gas" distribution, and the second as the "Mixed Gas" distribution.

In the central gas distribution, the dark matter will collide and pass through the gas, only interacting through gravitational forces. In this case, the gas does not collide with itself and any shocks or temperature changes will be caused by fluctuating gravitational forces. In the Central Gas distribution, the gas mixed in with each dark matter halo will collide with itself and cause strong shocks and an increase in temperature, due to the gas-on-gas collisions. There will also be the same element of gravitational interaction.

The gas and dark matter distributions were initially created separately. Fraser Smith set up the Dark Matter distributions, as well as the distributions with mixed dark matter and gas, using NFW profiles. The gas distribution was made spherical with a truncated $\frac{1}{r^2}$ density profile. Once this generating code had been developed it was incorporated into the initial conditions file writer for GIZMO. These particle positions were created and edited to contain the appropriate information on their mass and initial energies, and then this file was run through an "Evrard Collapse" using the GIZMO code. This led to the distribution seen in Figure 2.4. Fraser Smith provided a distribution of the two dark matter halos, which were then combined with the central gas distribution to create the distribution seen in Figure 2.5. He also created the initial conditions distribution of the dark matter halos and gas intermixed.

2.1.1 CREATING A HOT GAS DISTRIBUTION

The hot gas distribution was created first from a three dimensional grid of size $N \times N \times N$. $\frac{N}{2}$ was taken as the radius of the sphere, and any particles "outside" this

radius were discarded. The remaining particles then had their distances scaled so that the distribution would follow a $\frac{1}{r^2}$ distribution. This was done by taking the radius of each particle (called r_{val} and scaling it down to it's new value:

$$r_{new} = (\frac{r_{val}}{R})^3 \times R$$

The size of the grid used for the simulations was determined by the approximate number of particles needed. Each of the two distributions were tested at three different resolutions. In simulations, this means three different amounts of particles. The particle counts for the gas spheres were made to be approximately 30,000, 300,000 and 3,000,000. The grids used for the two different resolutions were $40 \times 40 \times 40$, $84 \times 84 \times 84$, and $142 \times 142 \times 142$ with particle counts of 33,371, 309,933, and 3,155,961, respectively. One can see that this is less then 40^3, 82^3, and 182^3 by a factor of about 0.5 due to particles outside the sphere's radius being removed.

To get these values, the equation for the volume of a sphere was used. Let's say one wants to find a radius that generates approximately 3000 particles.

$$V_{spere} = \frac{4}{3}\pi R^3$$

Now let's say the desired particle count is proportional the volume. We can rearrange to find the radius:

$$R = \sqrt[3]{\frac{3}{4\pi}V_{spere}}$$

Now one can find the desired R value given the particle count. Since R is half the diameter, and the diameter is what one would use to find the volume (or in this case, particle count) of the cube containing the sphere, one can also rearrange the equation into this form:

$$V_{spere} = \frac{4}{3}\pi D^3(\frac{1}{8})$$

$$V_{spere} = \frac{\pi}{6}V_{cube}$$

And $\frac{\pi}{6}$ rounded to the nearest decimal is 0.5.

Once this generating code was finished, it was used to create an initial conditions file for GIZMO, given a grid size. This needs to be handled carefully as the file formats for GIZMO expect specific ordering of data arrays. For example particles of given type (whether dark matter, gas, or stars) must be ordered within the file with gas particles first, dark matter second and star particles third. This conversion also involved adding data for the masses, initial velocities, and energies to the particles.

A file was generated for each resolution, and then individually run through an Evrard Collapse simulation using GIZMO. This simulation takes the hot gas distribution and lets it collapse under it's own gravity until it reaches equilibrium. The final distribution for the 182x182x182-grid case can be seen in Figure 2.1. This generated a file for a stable ball of hot gas that could then be used as the central gas in our first distribution.

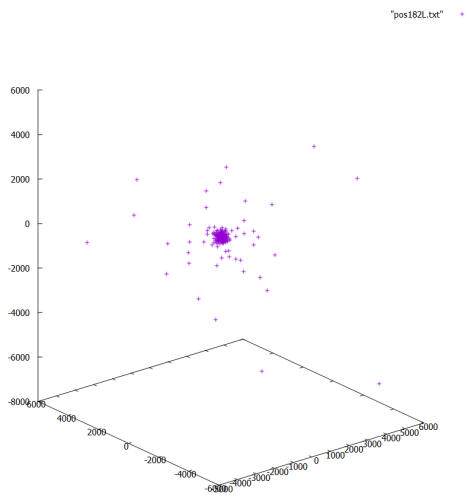

Figure 2.1: A scatter plot of one of every 1000 final positions for the 182x182x182 Evrard Collapse.

Figure 2.2 plots the internal energy over time of the three different Evrard Collapse simulations, while 2.3 plots the kinetic energies. It's important that the internal energies are within 5% of each other by the end of the simulation, so that when these distributions are used in the initial conditions files for the different resolutions, they have approximately the same starting energies. One can also see that the three graphs are showing asymptotic behavior with the higher resolutions, where they are approaching an "ideal" graph. This is a good sign that the evolution is converging with higher resolutions.

2.1.2 DARK MATTER SEPARATED FROM A CENTRAL GAS DISTRIBUTION

Fraser Smith provided distributions of dark matter halos, that were then offset from each other, with resolutions of 30,000, 300,000, and 3,000,000 particles. These were

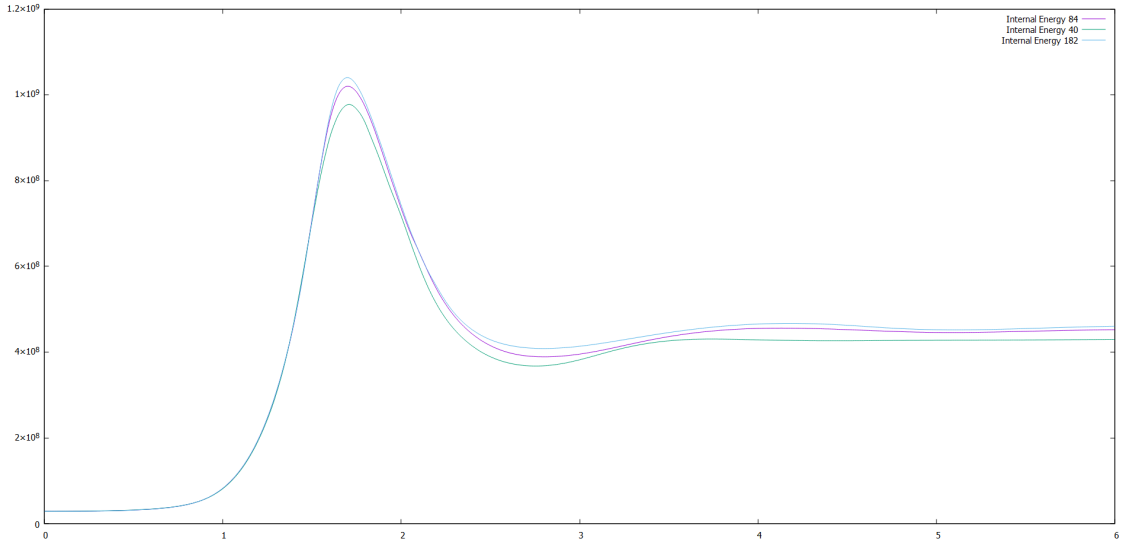

Figure 2.2: A comparison of the internal energies of the three different resolutions of the Evrard Collapse simulation.

developed by Fraser using GalactICS code and the MakeNewDisc package by Dr. Volker Springle. (12) The dark matter haloes are modeled with Herniquest profiles, which are designed to be approximately equivalent to NFW profiles within the virial radius. NFW profiles (or Navarro-Frenk-White profiles) are commonly used Dark Matter mass distributions for cold dark matter halos that are modeled from N-body simulations by Navarro, Frenk and White (8). The stellar and gaseous parameters were set to have zero mass and zero particles, and the dark matter's concentration was set to 6.0. The mass was set to be

$$10^{14}\frac{\Omega_{dark}}{\Omega_{matter}}M_{\odot}$$

Where $\Omega_{dark} = 0.25$ and $\Omega_{matter} = 0.30$, and $M_{\odot}$ is the symbol for solar mass.

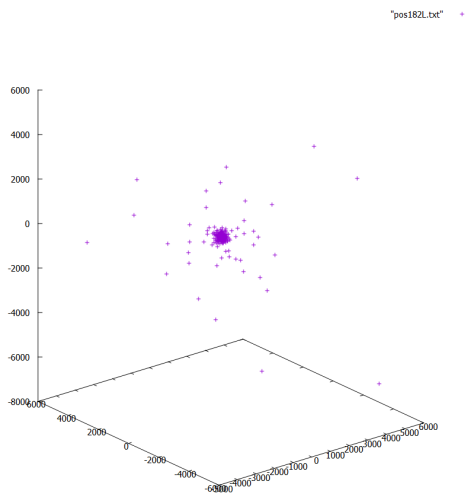

Figure 2.3: A scatter plot of one of every 1000 final positions for the 182x182x182 Evrard Collapse.

Code was then provided that can be used to combine a gas distribution with a dark matter distribution, and duplicate and offset the halos. This code was used so that the hot gas distribution was combined with Fraser's dark matter file to create the joint distributions with dark matter offset from a central gas. A graph of 1 of every 1000 particles of this distribution is shown in Figure 2.4. This combined distribution was then used as the initial conditions file to run the simulations in GIZMO.

2.1.3 DARK MATTER AND GAS DIRECTLY OVERLAID

Fraser Smith also developed and provided dark matter halos combined with gas in a mixed distribution, which were then offset from each other. The process for creating the dark matter halos was the same as before, except their mass was set to $10^{14} M_{\odot}$. Fraser created a FORTRAN code to add the gas to the dark matter in shells, with fail-safes ensuring none of the particles overlapped with each other. The

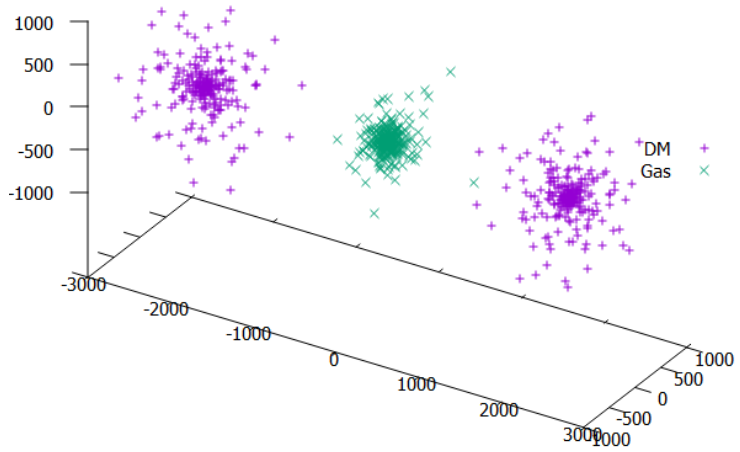

Figure 2.4: A scatter plot of the distribution with a central ball of gas and two dark matter halos.

gas distribution was a NFW distribution with the same concentration as the dark matter, and extending to the same virial radius. The mass of the gas was set so that $\Omega_{baryon} = 0.05$, keeping $\Omega_{matter} = 0.30$, the same ratio as before. Any mass from the gas was subtracted from the dark matter, to keep the overall mass at $10^{14} M_{\odot}$.

These files were then used as initial conditions for the runs with the dark matter and gas directly overlaid. See Figure 2.5.

2.2 SIMULATION CODE

GIZMO is a multi-physics simulation code that can be used for both collision-less and hydrodynamic systems that can be run on massively parallel cores. It is formed

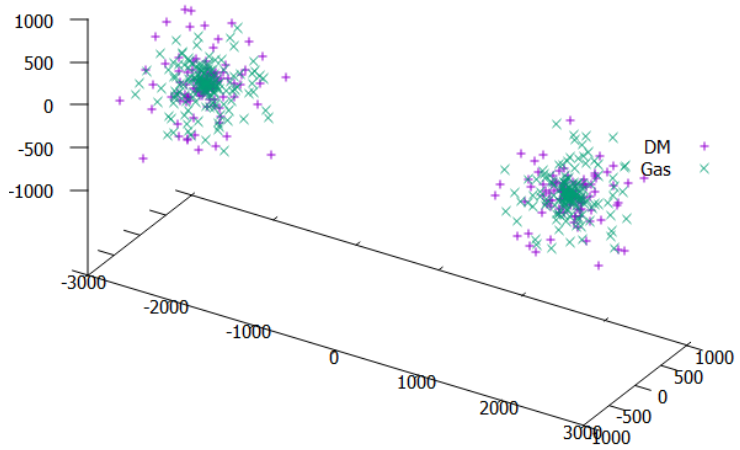

Figure 2.5: A scatter plot of the initial distribution of the two balls of dark matter and gas mixed together.

from the GADGET code, and is compatible with GADGET and uses similar naming conventions. (6) All of the simulations for this paper were run using GADGET on 8, 16, 32, and sometimes 64 cores on the SMU Computational Astrophysics Labratory, using MPI as the parallel platform. The longest simulation was the 3,000,000-particle Evrard Collapse. It took two weeks to complete, running on 64 cores. Originally, there was a concern that the 6000k particle runs would have taken months to complete, which was not feasible for the time frame of this thesis. However, the simulations ran much faster after adjusting the softening numbers for the number of particles present, and the 6000k particle simulations only took about 6 days to complete.

2.2.1 GRAVITY

GIZMO has code for self-gravity that is virtually identical to the original GADGET code. (6) GADGET and GIZMO use a Lagrangian Tree-PM method for calculating gravity. Tree-PM is a lagrangian particle-based method, and is efficient for running simulations where particles move on different time-steps. It separates the gravitational force into two components, and uses a gravity tree for the short range component, and a particle-mesh for the long range component (2).

2.2.2 HYDRODYNAMICS

The hydrodynamic suite for GIZMO seeks to combine the strengths of both the Adaptive Mesh Refinement method of simulating hydrodynamics and the Smoothed-Particle-Hydrodynamics method. GIZMO uses a weighting function that determines the way a particular volume is divided into kernels. This allows the volumes to adjust their own "resolution" at sharp edges. Velocities of individual particles are also chosen as the fluid momentum integrated over the volume associated with the particle. This allows GIZMO to avoid issues with other hydrodynamics codes that use AMR or SPH, such as AMR's loss of angular momentum or growing errors along grid-lines, and SPH's need for a large amount of "neighboring" particles in order to maintain accuracy (6).

Chapter 3

Results

3.0.1 Central Gas Distribution

The first distribution we will examine is the one with two dark matter halos offset from a central gas, as shown in Figure 2.4. This distribution starts at rest, with a centre of mass set to (0,0,0). Before starting the run, the drift velocity of the center of mass of the gas and dark matter were set to zero. Since we have two dark matter halos on either side of the central gas, the central gas is situated in an area with an unstable Lagrange point. Any drift or movement away from the centre of mass of the overall distribution, will cause the gas to be drawn to one of the halos over the other at an increasing rate.

Although this configuration is not likely to occur naturally, as most of the distributions we see in the cosmos are mixtures of dark matter and gas, studying this collision type is still valuable, as it allows us to more directly analyze the energy transfer between the dark matter halos and the central gas. The central gas is in hydrostatic equilibrium at the start of the simulation. It's thermal and kinetic energies have settled. Then, with the introduction of Dark Matter and the subsequent collisions, some of the dark matter's kinetic and potential energy is transferred into the gas.

As we shall see, the gas is indeed drawn to one of the dark matter halos over the other in each of our central gas configuration runs. This is not a desired result, as it would have been a simpler analysis if the collision was symmetrical across the x-axis. As is, particles move in a way that is still fairly symmetrical across the y and z axis of the distribution, but across the axis of collision, (defined as the x-axis) there is asymmetry, as the gas leaves the centre and collides with one halo early, oscillates back and forth around the centre of the distribution at x=0, and then when settling around 16 Gyrs is offset from the centre by about 100 kpc. The collision unbinds some of the outlying gas and dark matter particles, including a few at very high velocities that end up offsetting the centre of mass. Even when neglecting these far-off particles, there are still some gas particles in the outer region, around 3000 kpc from the centre, that are offset from the centre and skew the centre of mass.

Because of this behavior, it is important to factor in the movement of the dark matter and gas centre of mass of the central gas configuration in order to analyse the energies. This is not necessary in the Overlaid gas configuration run, which we will analyze in the next section, as the centre of mass of the dark matter and gas stays more or less at the exact centre of the distribution the entire run, and is symmetrical across the x axis.

The evolution of the dark matter kinetic and potential energy is given in Figure 3.1, and the gas kinetic, potential, and thermal energy in Figure 3.2.

We can immediately compare the energy between resolutions, and see that there's a surprising result in that the low and high particle resolutions have energy development that's much closer than the medium resolution run. This was unexpected, the expected result was that the medium resolution would be closer to the high resolution then the low resolution. However, what we are analysing in this paper is the energy transfer between the dark matter and gas, and the start and end values for the energies are what are most important to get out of these runs. And fortunately, in that aspect, the medium resolution run is actually much closer to the end results of the high resolution run. This particular configuration is also more complex to set-up than the overlapping gas runs and may have subtle differences in particle positions at one resolution compared to another.

The evolution of the dark matter energies can be seen in Figure 3.1. The dark matter slowly gains more and more kinetic energy as it accelerates towards the centre of the distribution. Then at around 8.4 Gyr, there's a shoulder in the kinetic and potential energy graphs. This is due to the central gas moving from the centre of the distribution and colliding with one of the halos early, causing that halo to briefly decelerate due to the shift in gravitational pull from the gas. Once the gas joins this halo though, the acceleration continues until the two halos collide at around 8.9 Gyr, and then there's a loss in kinetic energy as the gas and dark matter combine and settle at the centre of the distribution. There are some small bumps in the graph after this point, showing collisionless oscillations of the dark matter around the centre of mass.

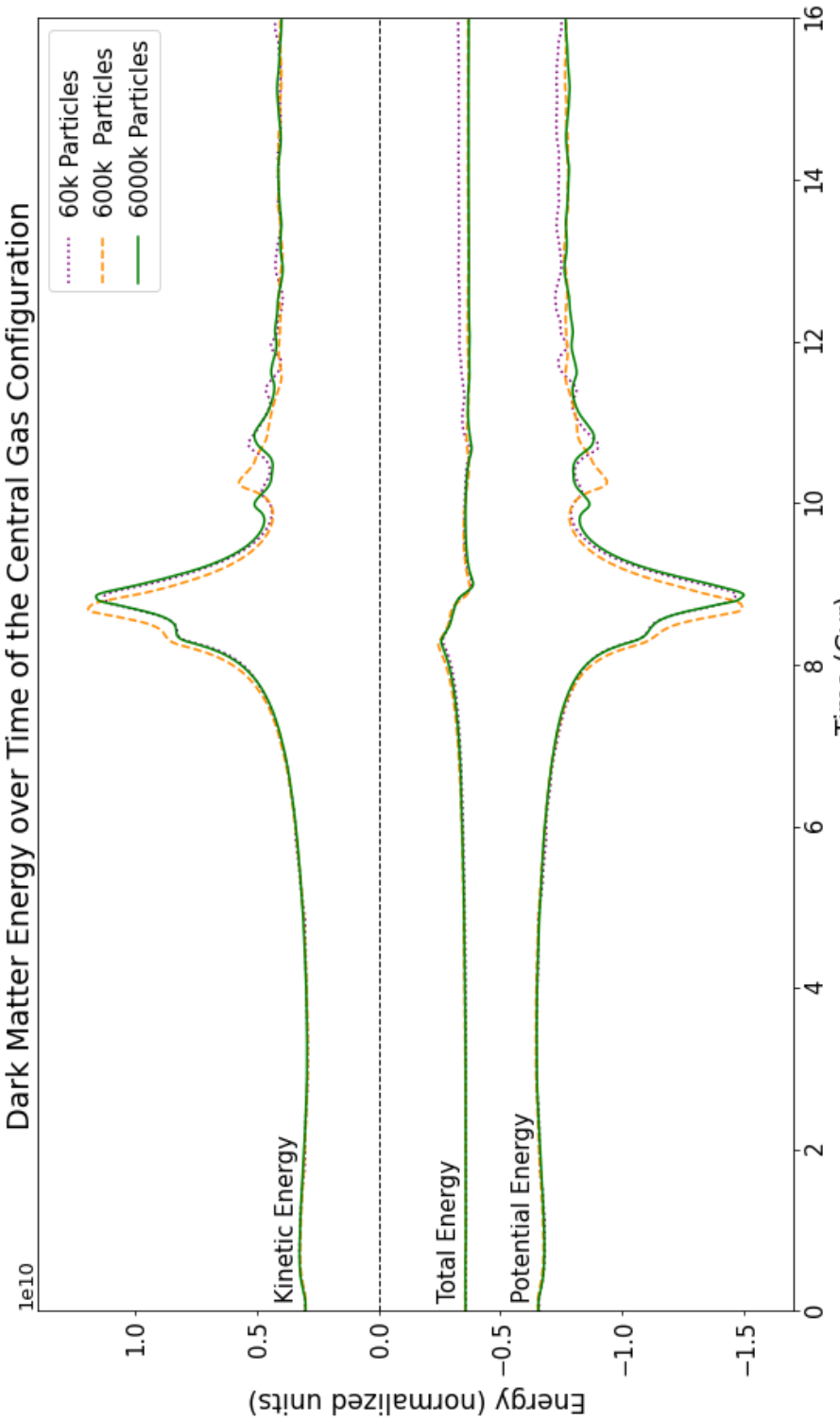

Figure 3.1: Potential and kinetic energies of the dark matter over time, of the Central Gas Configuration

The evolution of the gas energies can be seen in Figure 3.2. The potential energy of the gas can be seen to have two troughs. The lowest points of these troughs are at 8.3 and 8.8 Gyrs. These troughs line up fairly closely with peaks in the thermal and kinetic energy of the gas, as well as in the kinetic energy of the dark matter. As we can see by looking at the particle positions and centres of mass at these moments, these are the points at which the gas collides with the dark matter.

The centre of mass of the dark matter and gas over the 81 snapshot files is plotted in 3.3. The x-axis was used, as this is the axis the movement and collision occurs upon, and the y and z axes of this configuration are symmetrical except for small statistical variances. From analysing the positions of the dark matter centre of mass and gas centre of mass, we can see that the centre of the mass of the gas reaches it's maximum distance from (0,0,0) at around 8.3 Gyrs, exactly when the shoulder occurs, as well as the first peaks and troughs in the thermal, kinetic, total and potential energies of the gas. This is the point when the gas centre of mass collides with the first halo, and a position graph of this event can be seen in Figure 3.4a. This collision briefly slows the dark matter, and simultaneously the centre of mass of the gas is dragged to a stop by the gravitational pull of the dark matter halos. The gas centre of mass decelerates and changes direction, joining with the first halo to accelerate again and collide with the second at about 8.8 Gyrs. We can see this in Figure 3.3 as the approximate point when the dark matter and gas centre of masses intersect, with the closest position graph we have, for 8.9 Gyrs, shown in Figure 3.4b. The gas then overshoots, slowing to a stop at around 10.1 for the high resolution run, passing through the two halos

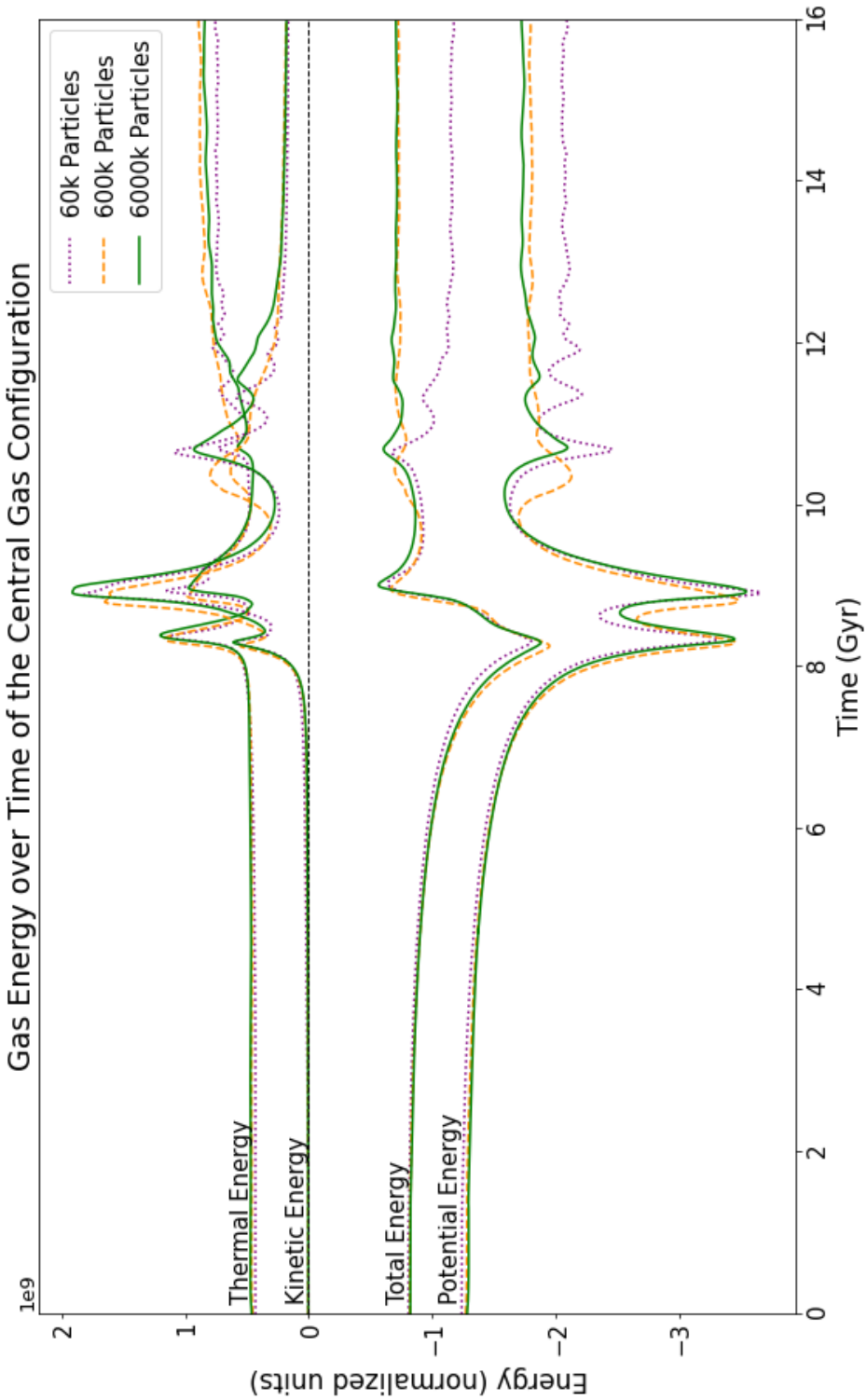

Figure 3.2: Potential, thermal, and kinetic energies of the gas over time of the Central Gas Configuration.

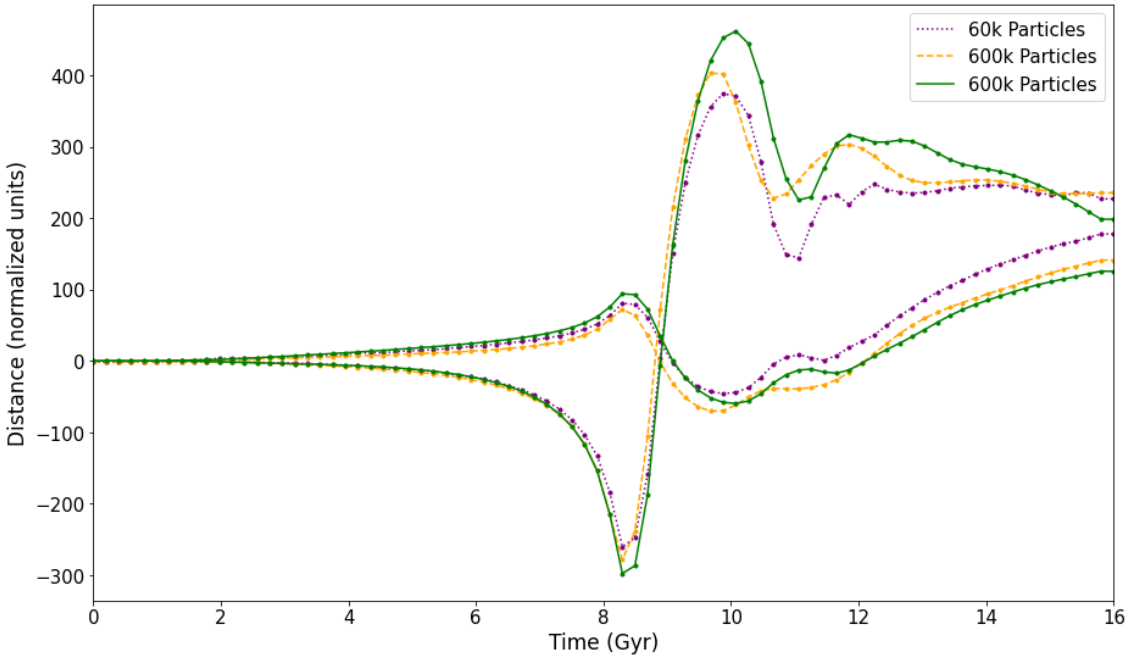

Figure 3.3: The distance in the x-direction of for the centre of the dark matter and gas, plotted over time. Each dot represents the centre of mass of one of the snapshots.

and then being pulled back for a third collision at 10.6 Gyrs, as seen in Figure 3.4d.

The thermal energy sees three spikes, around 0.01 - 0.03 Gyrs later than the local extremes in the kinetic and potential energy, and then a slow climb into a plateau. The kinetic energy of the gas also ends at a higher value then where it began. The ratio of the kinetic energy within a radius of 3000 kpc from the centre is 0.1 to 1 for the lowest resolution CGC run, and 0.2 to 1 for the medium and high CGC runs.

The collision we are calculating is by definition a closed isolated system. The maximum total energy should be more or less constant due to conservation of energy, and the energy statistics from our simulation code shows the total energy is constant to approximately 1% for the lowest resolution run, with higher resolutions having progressively better energy conservation. Hence we can analyse the energy transfer

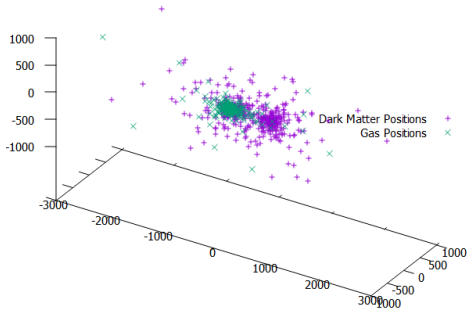

(a) Collision 1 (8.3 Gyr)

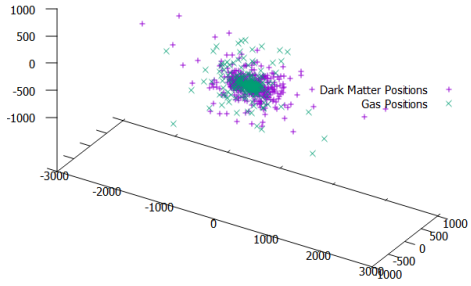

(b) Collision 2 (8.9 Gyr)

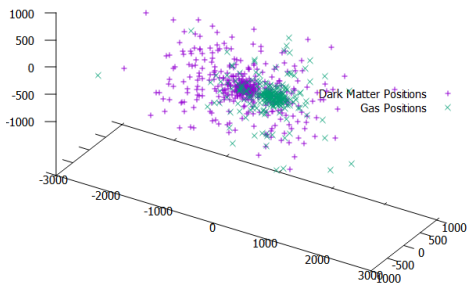

(c) Overshoot (10.1 Gyr)

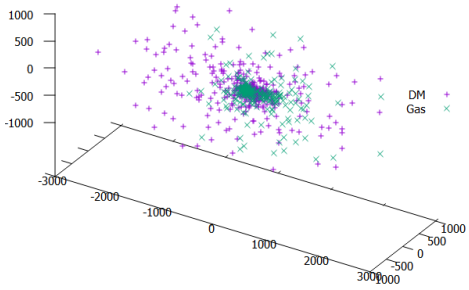

(d) Collision 3 (10.6 Gyr)

Figure 3.4: A scatterplot of the particle positions of the high resolution CGC run during each of the main collision events.

from the collision, by looking at where the energy values have settled before and after it occurs. In tables 3.1 to 3.3, we provide the energy values, normalized as a ratio of the initial total energy, of the each sector in turn. Together with our energy graphs and position data, we analyse the relative energy transfer.

The first item of note is that there's an increase to the thermal energy for each of the CGC runs, ranging from 0.0732 of the total energy, to 0.01 of the total energy.

Table 3.1: Energy data for the low resolution CGC run, as a ratio of the initial total energy of the system.

Energy Type	Start Energy	End Energy	Energy Difference	% Energy Increase
Thermal	0.10	0.17	0.07	75.09
Gas Kinetic	0.00	0.04	0.04	27528.11
Gas Potential	-0.28	-0.48	-0.19	68.58
Gas Total	-0.18	-0.27	-0.08	45.24
Dark Kinetic	0.69	0.96	0.27	39.45
Dark Potential	-1.51	-1.71	-0.20	13.29
Dark Total	-0.82	-0.74	0.07	-8.84
Total Kinetic	0.69	1.00	0.31	44.76
Total Potential	-1.79	-2.18	-0.39	22.01
Total Energy	-1.00	-1.01	-0.01	1.12

Table 3.2: Energy data for the medium resolution CGC run, as a ratio of the initial total energy of the system.

Energy Type	Start Energy	End Energy	Energy Difference	% Energy Increase
Thermal	0.10	0.20	0.10	96.89
Gas Kinetic	0.00	0.04	0.04	36310.56
Gas Potential	-0.29	-0.41	-0.12	41.32
Gas Total	-0.19	-0.17	0.02	-11.44
Dark Kinetic	0.68	0.92	0.23	34.15
Dark Potential	-1.50	-1.76	-0.26	17.44
Dark Total	-0.81	-0.84	-0.03	3.38
Total Kinetic	0.68	0.96	0.28	40.22
Total Potential	-1.79	-2.17	-0.38	21.32
Total Energy	-1.00	-1.01	-0.01	0.60

Table 3.3: Energy data for the high resolution CGC run, as a ratio of the initial total energy of the system.

Energy Type	Start Energy	End Energy	Energy Difference	% Energy Increase
Thermal	0.10	0.19	0.09	82.64
Gas Kinetic	0.00	0.04	0.04	38129.09
Gas Potential	-0.29	-0.39	-0.10	34.26
Gas Total	-0.19	-0.16	0.03	-14.22
Dark Kinetic	0.68	0.90	0.22	32.87
Dark Potential	-1.49	-1.75	-0.25	17.01
Dark Total	-0.81	-0.84	-0.03	3.74
Total Kinetic	0.68	0.94	0.26	38.80
Total Potential	-1.78	-2.14	-0.35	19.83
Total Energy	-1.00	-1.00	-0.00	0.37

In all resolutions this is essentially a doubling of the thermal energy of the initial configuration.

It's a natural question to ask, could this increase in thermal energy be due to the increase in the gravitational potential energy of the system from the added mass from the dark matter halos? An increase in mass and therefore gravitational forces towards the centre of the system could cause the central gas to collapse in further on itself, increasing the pressure and thermal energy of the gas. While it is tempting to consider whether this could be explained by adiabatic compression, the loss of outlying parts of the gas distribution makes an exact calculation difficult.

However, looking at the scatter plots and density distribution before and after the collision (as seen in figure 3.6 and 3.7), we can see that there is in fact a decreased density around the centre at the end of the run, and the ball of gas has expanded outwards. The increase in volume suggests a significant increase in pressure.

The energies were normalized by taking each value as the ratio of the initial total energy. The resulting energy values can be found in Tables 3.1, 3.2, and 3.3. The energy values referred to are all ratios with the initial total energy of their respective run, and all can be located in these tables.

For the low resolution run, the potential energy of the gas decreases by 0.0833, the decrease in the potential energy is larger than the increase to the thermal and kinetic energies. This energy is going into the dark matter, which is interesting, as the dark

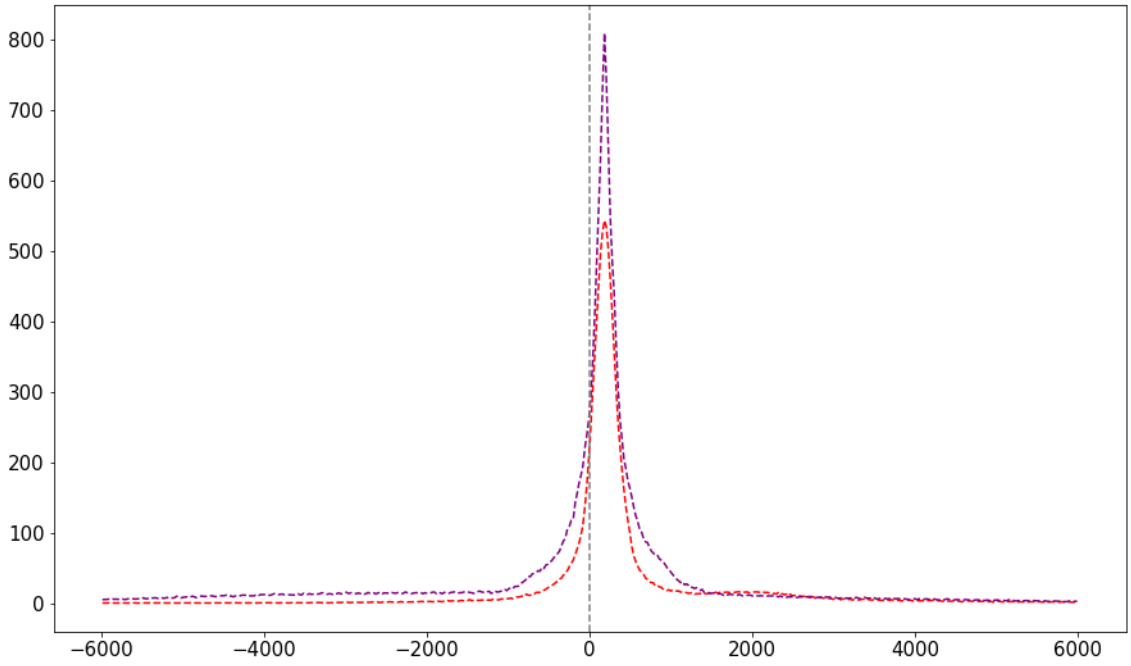

Figure 3.5: Linear density in x of the CGC gas particles at 16 Gyrs.

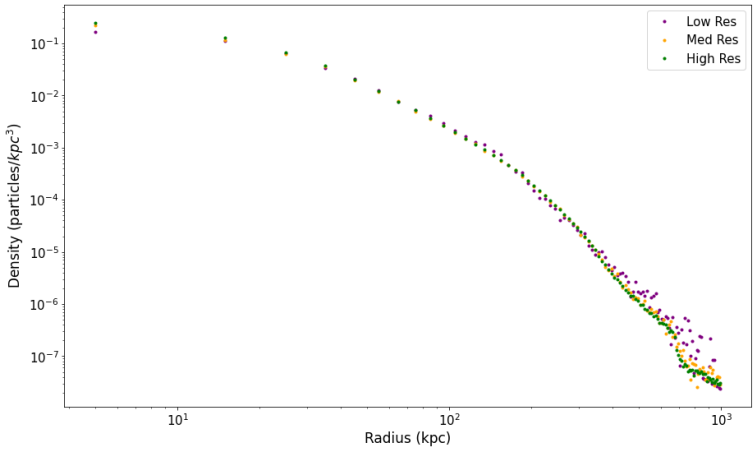

Figure 3.6: Initial Radial Density (as a loglog graph)

matter is initially what moves and collides with the gas, and then settles. If we had a stable Lagrange point and the gas was stationary throughout the collision, we likely wouldn't have seen this result. If we look at the total dark matter energy in Table 3.1, and compare it to the energy difference in the total energies, the Dark Matter has taken about 0.0721 of the kinetic and/or thermal energy of the gas.

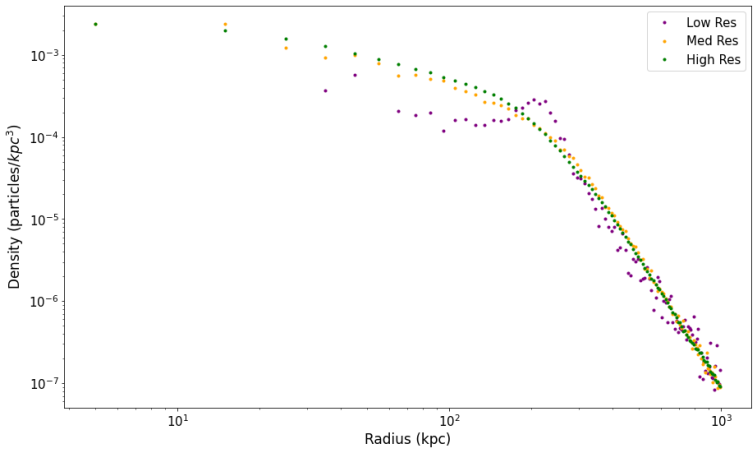

Figure 3.7: Final Radial Density (as a loglog graph)

However, for the medium and high resolution runs, the total energy of the gas increases by 0.0214 and 0.0216, respectively. This energy has to come from somewhere; and indeed, there's an approximate decrease in the total dark matter energy by 0.0275 and 0.0304, as well. The small difference here between the gas and dark matter values is the change in the total energy. The total energy should stay more or less constant through a run, while there is no set amount of variance that is required, in general as long as the change is less then 1% of it's total value a simulation is considered to have good accuracy. Which is true of each of our simulations, with the higher resolution and OGC runs being even more accurate (14).

Here, some of the kinetic energy of the dark matter is being converted into the thermal and kinetic energy of the gas, which is more along the lines of what was expected in a collision like this. If the potential energy decreases under virialization, then something else has to increase.

The main conclusion is that we do indeed see the energy being transferred into the gas in the medium and high resolution runs, but it is not easily predicted based upon changes in resolution due the sensitive nature of this particular run.

3.0.2 Dark Matter and Gas directly overlaid

The initial configuration of the dark matter and gas overlaid, starts with two dark matter halos mixed with gas, separated by a distance, as seen in Figure 2.5.

This configuration also starts at rest. The two spheres of dark matter and gas are drawn together by gravity. They accelerate and collide at the centre. When the gas collides with itself, it briefly becomes flattened perpendicular to the collision direction. The dark matter halos pass through the centre of mass, and then are drawn back in by gravity, and then the gas and dark matter expand and settle.

The initial configuration of the dark matter and gas overlaid, starts with two dark matter halos mixed with gas, separated by a distance, as seen in Figure 2.5. The graphs of the energy evolution's of the dark matter and gas, can be found in figures 3.8 and 3.9. Immediately one can observe the collision takes place at a later timestamp then for the previous distribution; a time of 12.8 is where the maximum kinetic energy of the gas and dark matter occurs, which is several time units longer then the maximum for the central gas distribution at 8.7. This is due to the gravitational force equation:

$$F = \frac{GmM}{r^2}$$

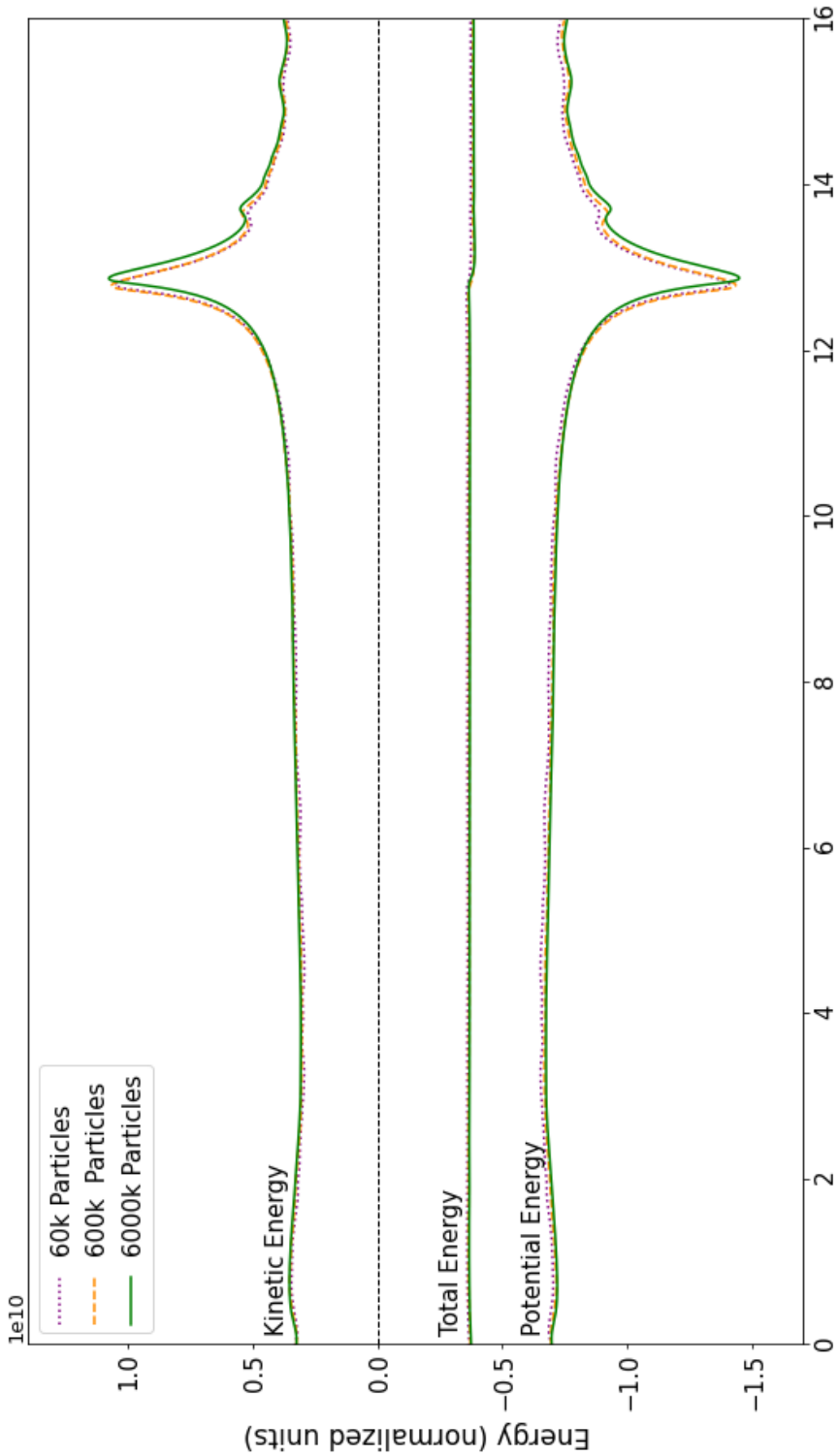

Figure 3.8: Potential and kinetic energies of the dark matter over time, of the Overlaid Gas Configuration

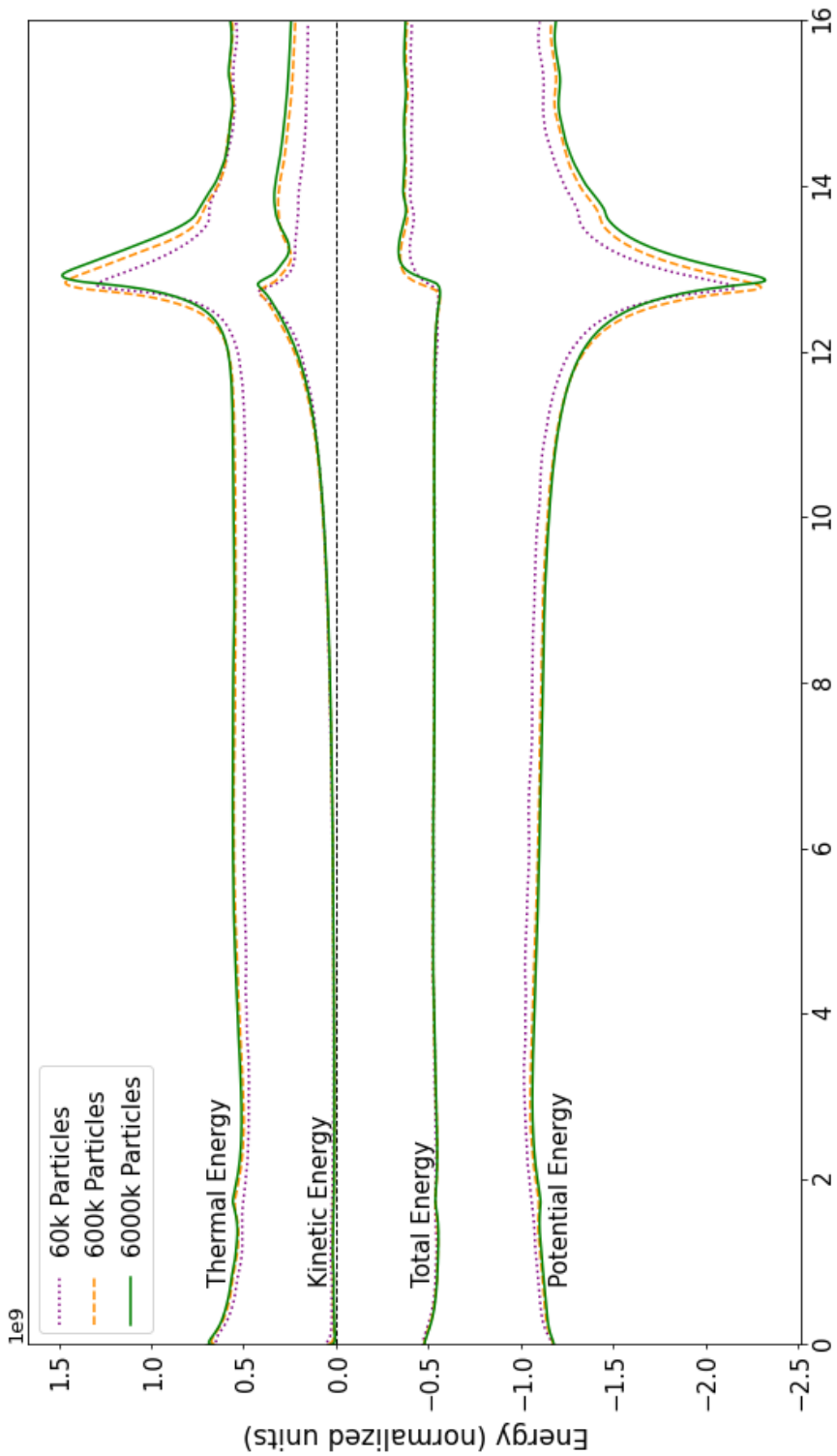

Figure 3.9: Potential, thermal, and kinetic energies of the gas energies over time, of the Overlaid Gas Configuration

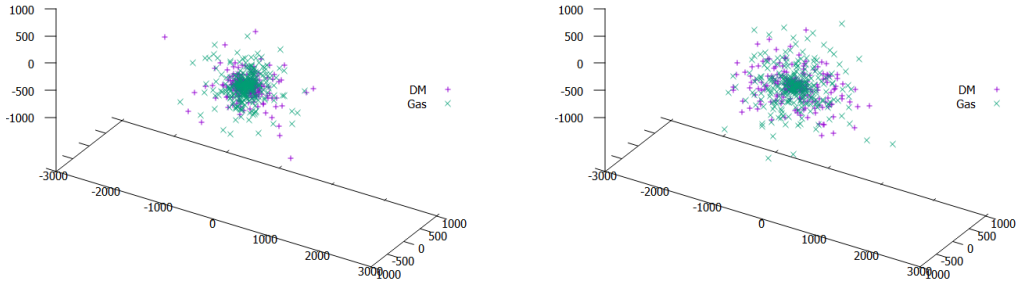

(a) Collision 1 (12.9 Gyr) (b) Collision 2 (13.7 Gyr)

Figure 3.10: A scatterplot of the particle positions of the high resolution OGC run during each of the main collision events.

The dark matter halos are the same distance apart, but the gas has changed location, intermixed with the dark matter halos, instead of being in the center of the distribution and contributing a gravitational force at half of the distance. Meaning, the acceleration starts off smaller and takes time to grow, and it takes longer before the collision happens. One can see the maximum dark matter kinetic energy is slightly higher for the central configuration.

The evolution of the energies and positions are simpler in the OGC run, as there's no central gas next to an unstable Lagrange point (although technically the Lagrange point still exists). The collision is fairly symmetrical across the x-axis (the axis of collision), and unlike the CGC run, the final density profile is centered closely to x=0, as can be seen in Figure 3.11.

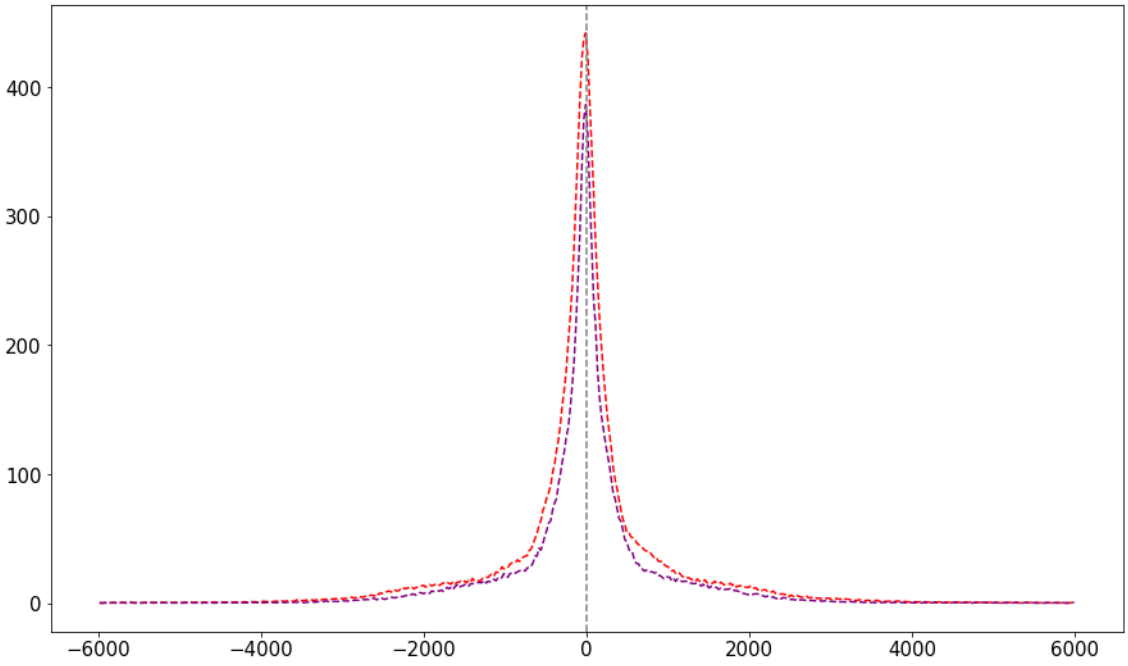

Figure 3.11: The linear density in x of the OGC positions at 16 Gyrs.

First looking at the dark matter energy evolution in Figure 3.8, we can see that the kinetic energy has one large peak at the collision, and then two smaller fluctuations afterwards. After the initial collision, the dark matter passes right through the gas and then slows as it is drawn back towards the centre of mass. The second peak is the second "collision", when the individual dark matter halos centre of mass accelerates again and meets the shared centre of mass of the system. The fluctuations of the CGC run are more numerous and larger in magnitude. This suggests that being mixed in with gas has a dampening quality on the dark matter distribution. In Pearce et al (9), it was discovered that balls of gas colliding with another ball of gas quickly reaches equilibrium, and has a dampening effect during collisions when mixed with dark matter. This is likely because the gas is collisional, so it reaches a maximum density while the dark matter moves through it, and is necessarily pulled back by this

configuration. The results in our paper suggest that the dampening effect is stronger when the gas and dark matter are already intermixed.

We can see that the fluctuations in the dark matter total energy are much smaller than in the CGC run as well. For the medium and high resolution runs, the total energy decreases a small amount during the collision, and then reaches a plateau. For the low resolution run, the dark matter total energy increases slightly after the collision, and also reaches a plateau, with a value slightly higher then it started with.

The gas energy evolution in Figure 3.9 shows a high peak in thermal energy during the collision.The thermal energy peak for the 60k particle run is the smallest, suggesting that the number of particles present affects the thermodynamics of the gas. The more particles there are the better the shock is resolved, hence a higher thermal energy. This also explains the lack of a second peak in the kinetic energy distribution for the low resolution run. Lower resolution inevitably means the second compression is less well captured. The high peak and in thermal energy, followed by a second peak in the kinetic energy after the collision (in the medium and high resolution runs) suggests that a shock occurred which propelled the movement of the gas. The 60k particle run didn't have this shock, but still had some adiabatic expansion and cooling of the gas.

The potential energy has a smooth trough, with small fluctuations in it's tail. There is a clear dependence on resolution here.

Table 3.4: Energy data for the low resolution OGC run, as a ratio of the initial total energy of the system.

Energy Type	Start Energy	End Energy	Energy Difference	% Energy Increase
Thermal	0.17	0.13	-0.04	-23.07
Gas Kinetic	0.00	0.04	0.04	inf
Gas Potential	-0.28	-0.27	0.02	-5.93
Gas Total	-0.11	-0.10	0.01	-12.47
Dark Kinetic	0.80	0.87	0.07	8.81
Dark Potential	-1.69	-1.77	-0.08	5.02
Dark Total	-0.89	-0.90	-0.01	1.61
Total Kinetic	0.80	0.91	0.11	13.38
Total Potential	-1.97	-2.04	-0.07	3.45
Total Energy	-1.00	-1.00	-0.00	0.02

Table 3.5: Energy data for the medium resolution OGC run, as a ratio of the initial total energy of the system.

Energy Type	Start Energy	End Energy	Energy Difference	% Energy Increase
Thermal	0.17	0.13	-0.03	-20.13
Gas Kinetic	0.00	0.05	0.05	inf
Gas Potential	-0.28	-0.28	0.00	-0.98
Gas Total	-0.11	-0.09	0.02	-18.94
Dark Kinetic	0.77	0.87	0.10	13.18
Dark Potential	-1.66	-1.78	-0.12	7.45
Dark Total	-0.89	-0.91	-0.02	2.49
Total Kinetic	0.77	0.92	0.15	19.97
Total Potential	-1.94	-2.06	-0.12	6.23
Total Energy	-1.00	-1.00	-0.00	0.06

We can also analyse the energies from before and after the collision here, to parse information about the energy transfer. The energy data for the OGC runs are in tables 3.4 to 3.6.

Immediately, we can see there is a consistent decrease in the thermal energy instead of the increase we saw in the CGC collision. The thermal energy decreased by 0.0391 in the lowest run, and 0.0310 in the highest resolution run. This is interesting, as in the OGC run, we have gas colliding with gas. It's likely here, the collision caused an

Table 3.6: Energy data for the high resolution OGC run, as a ratio of the initial total energy of the system.

Energy Type	Start Energy	End Energy	Energy Difference	% Energy Increase
Thermal	0.17	0.13	-0.03	-18.70
Gas Kinetic	0.00	0.06	0.06	inf
Gas Potential	-0.28	-0.28	-0.00	0.79
Gas Total	-0.11	-0.09	0.02	-21.34
Dark Kinetic	0.76	0.88	0.12	15.67
Dark Potential	-1.65	-1.79	-0.14	8.70
Dark Total	-0.89	-0.91	-0.02	2.71
Total Kinetic	0.76	0.94	0.18	23.19
Total Potential	-1.93	-2.07	-0.15	7.56
Total Energy	-1.00	-1.00	0.00	-0.01

increase in temperature and pressure initially, that resulted in the adiabatic expansion and cooling of the gas.

The kinetic energy of the gas has increased as well, from an initial value very close to zero. The kinetic energy increase ranges from 0.0365 in the lowest resolution run to 0.0574 in the highest run and shows a consistent trend of increasing with resolution. Another difference is the increase in the potential energy of the gas in the low and medium resolution runs, rather than a decrease. This is very interesting, as for these resolutions, the potential energy at the end of the run is marginally larger then it is at the beginning, with the mixed balls of gas and dark matter separated and attracting each other. This is likely due to the adiabatic expansion of the gas. Since the average radius of the gas particles from the centre of the distribution of the gas has increased, there is greater gravitational potential energy. It's likely the thermal dynamics of this process was impacted by the resolution, as the amount of potential energy difference decreases for each resolution until the highest, when it is negative. We can see in

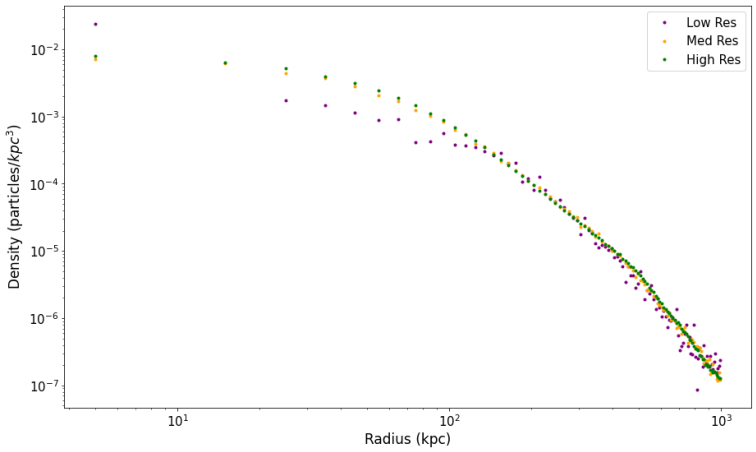

Figure 3.12: Final Radial Density of the OGC run (as a loglog graph)

Figure 3.12 the final loglog density distribution for the OGC runs.

The gas total energy has increased by about 0.0141 - 0.0241, just as the total energy of the dark matter has decreased by about 0.0143-0.0240. Energy from the dark matter is being transferred into the gas, just as for the medium and large CGC runs. It's very interesting to note, the total energy transferred into the gas of both the CGC and OGC runs is fairly close between the two high resolution runs. 0.0241 in the large OGC run, and 0.0267 in the large CGC run, a difference of about 0.0026.

Chapter 4

Conclusions

4.1 Main findings

1. In both collisions, energy was transferred into the gas, approaching approximately the same ratio of the initial total energy; 0.0241 in the OGC run and 0.0267 for the CGC run, with an exception in the low resolution CGC run, where energy was lost, with a difference in the initial and final total gas energy ratios of -0.0833. As the configurations of the gas and dark matter are so different, this is slightly unexpected, but highlights a clear trend of the collisionless material passing energy on to the collisional.

2. The gas being intermixed with the dark matter in the OGC run caused an increased dampening effect during the collision.

3. The OGC run's initial gas-on-gas collision caused a spike in temperature that lead to increased adiabatic expansion of the gas, and cooling.

4. The CGC run's collision was asymmetrical along the collision axis, due to an unstable Lagrange point, and the ball of gas was dragged towards one of the dark matter distributions, and then pulled back and forth.

The different configurations caused a large difference in thermal and kinetic energy transfer from the dark matter to gas, but the total energy transfer remained roughly the same. As we only had two different configurations, more research needs to be done to see if this result is repeatable with more configurations. But this suggests that the energy transfer between dark matter and gas remains roughly the same regardless of configuration, and what changes is the amounts transferred to the kinetic and thermal energies. Or results suggest that an intermixed distribution ends up having more energy transferred into kinetic energy, and a separate distribution ends up having more energy transferred into thermal energy.

4.2 Future work

It was unexpected that the energy evolution of the medium-resolution distribution didn't agree close with the energy evolution of the large resolution distribution, and it is likely that there is an issue with the initial conditions that needs to be addressed. It's possible there could be issues with the centre of mass and velocity. These issues likely tie in with the unstable Lagrange point, and although the Lagrange point can't be removed, small improvements could be made to get the centre of mass as close to zero as possible.

Some of these issues could also potentially be addressed with multiple copies of the distributions each created with a different random seed.

It would also be interesting to look at the unstable Lagrange point in the CGC run with these random seeds, and see what impact the starting centre of mass and velocity have, even when very close to zero.

It would be interesting to look at runs where the gas and dark matter are alone, to compare with the combined runs. One could expand this work by giving the dark matter and gas different starting velocities, and see if there is an upper limit to the energy transfer between the dark matter and gas. Collisions between more varied configurations that compare the energy transfer, and see if they also have an energy difference around 0.026-0.07, and what factors change what. Is it repeatable that there's a greater increase to thermal energy when the dark matter and gas are separated, and an increase to kinetic energy, and cooling, when they are mixed? Do the total energy transfer ratios change if the ratio of dark matter and gas particles change?

Bibliography

[1] Heinz Andernach and Fritz Zwicky. English and spanish translation of zwicky's (1933) the redshift of extragalactic nebulae, 2017.

[2] J. S. Bagla. Treepm: A code for cosmological n-body simulations. *Journal of Astrophysics and Astronomy*, 23(3–4):185–196, December 2002.

[3] Matthew Colless, Gavin Dalton, Steve Maddox, Will Sutherland, Peder Norberg, Shaun Cole, Joss Bland-Hawthorn, Terry Bridges, Russell Cannon, Chris Collins, Warrick Couch, Nicholas Cross, Kathryn Deeley, Roberto De Propris, Simon P. Driver, George Efstathiou, Richard S. Ellis, Carlos S. Frenk, Karl Glazebrook, Carole Jackson, Ofer Lahav, Ian Lewis, Stuart Lumsden, Darren Madgwick, John A. Peacock, Bruce A. Peterson, Ian Price, Mark Seaborne, and Keith Taylor. The 2df galaxy redshift survey: spectra and redshifts. *Monthly Notices of the Royal Astronomical Society*, 328(4):1039–1063, December 2001.

[4] Michael R. Blanton et al. Sloan digital sky survey iv: Mapping the milky way, nearby galaxies, and the distant universe. *The Astronomical Journal*, 154(1):28, June 2017.

[5] W. Freedman. Measurements of the hubble constant: Tensions in perspective*. *The Astrophysical Journal*, 919:16, 09 2021.

[6] Philip F. Hopkins. A new class of accurate, mesh-free hydrodynamic simulation methods. , 450(1):53–110, June 2015.

[7] Edwin Hubble and Milton L. Humason. The Velocity-Distance Relation among Extra-Galactic Nebulae. , 74:43, July 1931.

[8] Julio F. Navarro, Carlos S. Frenk, and Simon D. M. White. The structure of cold dark matter halos. *The Astrophysical Journal*, 462:563, May 1996.

[9] F. R. Pearce, P. A. Thomas, and H. M. P. Couchman. Head-On Mergers of Systems Containing Gas. , 268:953, June 1994.

[10] Vera C. Rubin and Jr. Ford, W. Kent. Rotation of the Andromeda Nebula from a Spectroscopic Survey of Emission Regions. , 159:379, February 1970.

[11] Barbara Ryden. *Introduction to cosmology*. 2003.

[12] Volker Springel. The cosmological simulation code gadget-2. *Monthly Notices of the Royal Astronomical Society*, 364(4):1105–1134, December 2005.

[13] R. J. Thacker, E. R. Tittley, F. R. Pearce, H. M. P. Couchman, and P. A. Thomas. Smoothed particle hydrodynamics in cosmology: a comparative study of implementations. *Mon. Not. Roy. Astron. Soc.*, 319:619, 2000.

[14] Peter Thomas and H. Couchman. Simulating the formation of a cluster of galaxies. *Monthly Notices of the Royal Astronomical Society*, 257:11–31, 06 1992.

[15] Edward J Wollack. Wmap big bang cmb test, Feb 2024.